Electric Power Systems Research 214 (2023) 108917

Contents lists available at ScienceDirect

Electric Power Systems Research

journal homepage: www.elsevier.com/locate/epsr

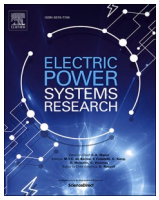

Techno-economic multi-objective reactive power planning in integrated wind power system with improving voltage stability

Abdelfattah A. Eladl [a,*], Mohamed I. Basha [b], Azza A. ElDesouky [c]

[a] Mansoura University, Faculty of Engineering, Electrical Eng. Department, Mansoura 35516, Egypt
[b] East Delta Electricity Production Company (EDEPCo), Ministry of Electricity, Damitta, Egypt
[c] Port-Said University, Faculty of Engineering, Electrical Eng. Department, Port Fouad 42526, Egypt

ARTICLE INFO

Keywords:
Reactive power planning
Wind energy
Uncertainty
VAR Sources
MOGA optimization
Voltage stability

ABSTRACT

Electrical power systems encounter a variety of challenges due to load growth and technological improvement; reactive power planning (RPP) and improvement of voltage stability (VS) are the two most significant ones. The integration of wind farms (WFs) into power networks has many advantages in terms of operation cost and emissions. But leads to voltage instability if it is not optimally sized, placed, and coordinated with VAR sources. In this study, a probabilistic multi-objective RPP framework is proposed for power systems with high penetration of WFs. A novel wind turbine model that can dynamically control reactive power is suggested based on the capability curve of a double-fed induction generator. A new bi-level optimization technique is introduced to address the problem considering the uncertainties of loads and wind power. Multi-objective genetic algorithm is employed at the upper level to optimally allocate VAR sources, and select the optimal locations of WFs to improve VS and decrease VAR sources' costs. While at the lower level, the overall operation cost is minimized. A fuzzy min-max method is modified to find the optimum compromise solution. The results show that the proposed technique is effective in improving system VS and operation costs.

1. Introduction

1.1. Motivation

The electrical sector has historically been focused on hydroelectric and thermal power plants. While hydroelectric plants are clean and effective, there is a constraint on locations for their installation. The fossil fuels required for other plants, on the other hand, are running out and are considered one of the main causes of CO_2 emissions. This has led to a significant shift in the paradigm of power systems, with governments adopting goals and strategies targeted at the comprehensive incorporation of renewable energy into electricity networks. Wind power stands out among other green energy because it has enhanced the convergence of networks greatly [1]. In recent years, wind power technology has evolved rapidly. In 2021, the installed wind power capacity grew by 92 GW, taking the global total installed capacity to 837 GW. The Global Wind Energy Council predicts that by 2025, the sector will expand rapidly and step upward to achieve a total installed capacity of 1014 GW [2].

The nature and operations of the power system are challenged by the fluctuating nature of the wind and the relatively new types of generators, such as double-feed induction generators (DFIGs), which are utilized in wind farms (WFs) but are uncommon in conventional power systems [3]. As a result, a large proportion of wind penetration may have an impact on the power grid's stability [2], necessitating proper reactive power planning (RPP) to keep the system operating safely.

1.2. Literature review

RPP, which is one of the most important aspects of the above challenging situation, is concerned with addressing the following two questions: (1) where the new reactive power sources should be implemented; and (2) the scale and form of the new reactive power sources. An adequate RPP can improve both the voltage profile and the voltage stability (VS) of the power grids. Many control behaviors (control variable) can have an effect on the RPP issue rather than depending on new sources such as: (i) Regulating the generator excitation is used to adjust the voltage set points of voltage-controlled buses (PV buses or generator voltage). (ii) Updating the configuration of taps for changing transformers. However, in the majority of power networks, these two strategies are insufficient due to high system stress. Capacitor banks, on the

* Corresponding author.
E-mail address: eladle7@mans.edu.eg (A.A. Eladl).

https://doi.org/10.1016/j.epsr.2022.108917
Received 30 July 2022; Received in revised form 6 October 2022; Accepted 19 October 2022
Available online 27 October 2022

Notation

Below is a list of the most important symbols used in this work. As needed, other symbols are defined

A	Sets of indices
N_b	Number of system buses
N_{cap}	Number of newly installed capacitor bank
N_g	Number of generators
N_L	Number of transmission line
N_s	Number of loads scenarios
N_{SVC}	Number of newly installed SVC devices
N_T	Number of installed transformers
N_{TCSC}	Number of newly installed TCSC devices
N_w	Number of installed wind power farmsB

Constants and parameters

B_{ij}	Susceptance of the branch between bus i and bus j (p.u)
C_c	Capacitor bank per-unit cost ($/MVAR)
C_F	Fixed cost of the capacitor bank in ($)
G_{ij}	Conductance of the ranch between bus i and bus j (p.u)
ir	VAR devices interest rate (%)
LT	VAR devices lifetime (years)
P_{Dmax}	The maximum possible power transfer to the load (MW)
P_{Gi}^{min}, P_{Gi}^{max}	Minimum and maximum allowable active power at bus i (MW)
Q_{Gi}^{min}, Q_{Gi}^{max}	Minimum and maximum allowable reactive power at bus i (MVAR)
S_l^{max}	Maximum allowable apparent power in line l (MVA)
T_K^{min}, T_K^{max}	Minimum and maximum transformer K tap setting limit (p.u)
V_i^{min}, V_i^{max}	Minimum and maximum allowable operating voltage at bus i (p.u)
X_{ij}	Branch reactance between bus i and bus j (p.u)
Z_{ij}	Branch impedance between bus i and bus j (p.u)C

Variables

AIC_{VAR}	Annual cost of newly added VAR sources ($)
$B_{svc.i}$	Susceptance of SVC device at bus i (p.u)
$C_{Cap.i}$	Total capacitor bank cost at bus i ($)
$C_{svc.i}$	SVC devices installing cost at bus i ($/MVAR)
$C_{TCSC.l}$	TCSC devices installing cost in line l ($/MVAR)
IC_{VAR}	Total new VAR sources installing cost ($)
P_D	Current load demand operating value (MW)
P_{Di} . Q_{Di}	Active and reactive power load at bus i (MW/MVAR)
P_{gi} . Q_{gi}	Active and reactive power generated at bus i (MW/MVAR)
Q_{ci}^{o}	VAR source capacitive/inductive power at bus i (MVAR)
$Q_{svc.i}$	SVC device reactive power injection at bus i (MVAR)
T_K	Transformer K tap setting (p.u)
S_l	Apparent power flow in line l (MVA)
$S_{TCSC.l}$	TCSC device power injections in line l (MVAR)
V_i . V_j	Magnitude of the voltage at bus i and j (p.u)
$X_{TCSC.l}$	TCSC device reactance in line l (p.u)
δ_{ij}	Phase-angle difference between bus i and j (rad.)

other hand, are the most common reactive power compensation solutions because they are fairly priced relative to their capability for compensation, but they also have the drawback of being slow and unreliable [1,4]. Flexible AC Transmission System (FACTS) is widely used in the power system due to its rapid control responses and capacity to boost loadability. Additionally, it creates new possibilities for regulating power flow, reducing losses, and boosting the unstable capacity of existing transmission lines [5].

Various artificial intelligence-based optimization methods have recently been used for the RPP with wind power integration. Authors in [1] suggested an application of the differential evolution particle swarm optimization algorithm (DEPSO) to minimize losses and VAR investment cost with wind power penetration. In [3], a differential evolution algorithm (DE) is presented to solve the RPP problem for 6 scenarios of different wind speed levels. In [6] the optimization problem was solved using a genetic algorithm (GA) with a static var compensator (SVC). The study in [7] presented an RPP method for integrating wind power into a distribution system. Tabu search was utilized to reduce the annual energy losses in the grid-connected system and improve the microgrid success index in [8]. The work in [9] proposed an improved adaptive GA for a multi-scenario expectation model using SVC. Adaptive GA was proposed in [10] to reduce the annual comprehensive cost using capacitor banks. Particle swarm optimization gravitational search algorithm (PSOGSA) was investigated in [11] to maximize the annual profit of the utility. Authors in [12] presented a multi-objective function model that takes into account minimal voltage variation, minimum active power losses, and maximum DG optimization capacity. However, no one in the preceding literature has focused on VS improvement as a crucial planning objective, instead focusing solely on minimizing losses and additional VAR costs.

In [13] a multi-scenario with two sets of variables was proposed and solved based on VS constrained optimal power flow method to minimize the total system cost. Two different objectives of minimizing the active power losses and VS index (named ʟ-index) were approached in [14], while VAR compensation devices were modeled as discrete variables. In [15], GA was proposed with a probabilistic model of wind turbine (WT), VS index was established as one of the multi-objective functions. In [16], a multi-objective algorithm was suggested, where the optimal compromise solution was found by combining the min-max technique, fuzzy decision maker, and ε-constraint method. However, they depicted the WT as a restricted PQ model, which prevented full utilization of the WT 's reactive power injection. In [17], a dynamic reactive power control strategy was used to model the WT, and multi-objective functions were merged as a single objective using the weighted method. GA was used to tackle multi-objective optimization problems. In [18], non-dominated sorting GA was proposed, and different strategies for controlling the reactive power of WTs on RPP were investigated. However, it should be emphasized that in [17] and [18], the rotor voltage limits in the wind power capability curve as well as the operational wind cost were ignored.

Recently, authors in [19] proposed a strategy for RPP with the objective formulated by measuring different cost components such as VAR generation cost, line charging cost, FACTS device operation cost, and cost due to real power loss. The work proposed in [20] integrates the static and dynamic solutions for the RPP problem in industrial microgrids operating in islanded mode. As a static solution, the optimal location of capacitors banks is determined to mitigate the voltage violations with demand increases. While the STATCOM as dynamic support is placed on the most sensitive bus to support fast voltage recovery under motors start-up states. An oppositional-based Harris Hawks optimization technique enthralled is suggested and implemented for RPP in [21] with the objective of minimizing the operation costs and transmission losses. To minimize power loss along with improvement in the voltage stability limit, the study in [22] proposed a Moth-flame optimization algorithm for RRP using multi-type of FACTS devices. Authors in [23] utilized a two-stage approach based on mixed integer linear programming for the RPP approach coupling steady-state operation and dynamic VAR demand resulting from intra-hour transitions as well as line-outage and short-circuit scenarios to a generic transmission system. However, all of these studies did not take into account the presence of renewable

energy sources within the system and the state of uncertainty for them, and the load demand.

In the present work, a bi-level optimization strategy is proposed to tackle the RPP issue. On the basis of the uncertainty characteristic of loads and wind power, a multi-objective genetic algorithm (MOGA) is employed in the upper stage to optimally assign new VAR sources and identify the best connecting locations of WFs in order to compensate for the shortage of reactive power in the power network. The objectives at this stage are to maximize VS and minimize the installation cost of new VAR sources. While the total fuel cost and WT operation cost are minimized as possible at the lower level. The MOGA solution process is a set of points on Pareto's optimum front, where the best compromise solution may be determined using a fuzzy min-max approach. Table 1 classified the surveyed literature and lists the suggested work's unique features in contrast to previous studies.

In the current work, to compensate and manage the reactive power in the electricity grid, several VAR resources are utilised. These are capacitor banks and FACTS devices. There are several types of FACTS devices that may be employed in a power network. Thyristor-controlled series compensators (TCSC) and SVC are two of the most appropriate devices for our requirements [5,24]. The model details of these VAR sources can be found in [25]. For static implementations, the modelling of VAR sources may be done through two methods: (i) the power injection model and (ii) the impedance insertion model. According to the impedance insertion model, depending on the kind of device, the impedance is injected into the system in series, shunt, or a mix of both.

Table 1
A comparison among previous studies and the proposed work novelties.

Ref.	Year	Optimization algorithm	Objective(s)	VAR sources Capacitors bank	FACTS	VS index	Wind model	Wind cost	Multi-scenario	Proposed multi-objective
[1]	2014	DEPSO	Min. cost of losses and VAR sources	✓	✓	–	Constant power factor	×	✓	–
[3]	2012	DE	Min. cost of losses and VAR sources	×	✓	–	Reactive power fixed band	×	✓	–
[6]	2006	GA	Min. cost of losses, VAR sources, and fuel cost)	×	✓	–	Reactive power fixed band	×	✓	–
[7]	2010	Quantum Evolution	Min. cost of losses and VAR sources	✓	×	–	–	×	✓	–
[8]	2014	Tabu search	Min. cost of losses and Max. microgrids success index	✓	×	–	–	×	✓	–
[9]	2016	Adaptive GA	Min. cost of losses and VAR sources	×	✓	–	–	×	✓	–
[10]	2018	Adaptive GA	Min. cost of losses and VAR sources	✓	×	–	Constant power factor	×	✓	–
[11]	2018	PSOGSA	Max. annual profit	✓	×	–	Constant power factor	×	×	–
[12]	2020	GAMS	Min. cost of losses and Min. voltage deviation and Max. DG capacity	✓	×	–	–	×	×	Weighted method
[13]	2014	GAMS & MINLP	Min. cost of losses and VAR sources with Max. VS	✓	×	VSM	–	×	✓	ε-constraint
[14]	2016	GAMS & MO—ORPD	Min. cost of losses and VAR sources with Max. VS	✓	×	L-index	Constant power factor	×	✓	Pareto optimal set and Fuzzy decision maker
[15]	2015	GA	Min. cost of losses and VAR sources with Max. VS	✓	×	L-index	–	×	×	Weighted method
[16]	2021	GAMS	Min. cost of losses and VAR sources with Max. VS	✓	×	L-index	Reactive power fixed band	×	✓	ε-constraint and Fuzzy decision maker
[17]	2013	GA	Min. cost of losses and VAR sources with Max. VS	×	✓	VSM	Dynamic reactive power control	×	✓	Weighted method
[18]	2019	NSGA	Min. cost of Fuel and VAR sources with Max. VS	✓	×	L-index	Dynamic reactive power control	×	✓	Pareto optimal set and Fuzzy decision maker
[19]	2022	DECSA	Min. cost of losses, VAR sources, FACTS, and line charging	✓	✓	–	–	–	–	–
[20]	2022	–	Min. cost of losses and VAR sources	✓	✓	–	–	–	–	–
[21]	2022	OHHO	Min. cost of losses, VAR sources and operation cost	✓	×	–	–	–	–	–
[22]	2022	Moth-Flame Optimization	Min. cost of losses and VAR sources with improve voltage profile	✓	✓	L-index	–	–	–	–
This paper		MOGA	Min. cost of Fuel and VAR sources with Max. VS	✓	✓	VSM	Dynamic reactive power control	✓	✓	Pareto optimal set and Fuzzy decision maker

GAMS: General Algebraic Modeling System.
MINLP: Mixed Integer Nonlinear Programming solver.
MO—ORPD: Multi-Objective Optimal Reactive Power Dispatch.
DECSA: Differential Evolutionary & Crow Search Algorithm.
OHHO: Oppositional-based Harris Hawk Optimizer.

The power injection model executes the VAR source as an element that injects/absorbs a specific quantity of active and/or reactive powers to a node. These techniques do not conflict with the symmetry of the admittance matrix and allow effective and easy incorporation of VAR sources into existing analytical software applications for the power system, which was used in this work.

1.3. Contributions and paper organization

This work focuses on RPP and improving the VS of the power system by installing new VAR sources which maximize the voltage stability margin (VSM) while keeping the minimum permissible voltage in mind with the high penetration of wind power. The system would be more capable of sustaining sufficient reactive power for running the network in a safe state with an allowable voltage level. As a result, the system would be more efficient in the face of wind power's fluctuating nature. Capacitor banks and FACTS which offer a rapid control response and the potential to enhance system loadability are utilized as VAR sources to support the network. To test the effectiveness of the suggested technique, an updated IEEE 30-bus test system and a part of the electricity grid in South Egypt are employed.

A detailed model is utilized to describe wind generators instead of the traditional technique in which wind generators were given in power flow studies as PV or PQ models with constant power factors [17]. This technique appears to be relatively simple so far, however, the reactive power range accessible is restricted to either a maximum power factor or a predetermined regulatory band. Furthermore, because this representation is not quite accurate, the reactive power infusion from the WT is not fully used.

The WT model studied in this work takes into consideration all available reactive power and provides dynamic reactive power control. A WT generator's output is non-linearly proportional to wind speed; therefore, it can vary from zero to its rated output when the wind speed fluctuates. As a result, these uncertainties should be accounted for in the power flow model. A probabilistic model is an ideal representation for addressing this issue. Because of its stochastic nature, the available wind energy is estimated using the Weibull distribution function, while the conventional Gaussian probability distribution function (PDF) is used to describe the load demand. Furthermore, the proposed strategy takes into account the unpredictability of wind power by integrating variables for overestimation and underestimation of available wind energy in the wind cost model.

The main contributions of the present work can be summarized as follows:

- A probabilistic multi-objective framework of the RPP problem is suggested for power networks with high wind energy penetration.
- A novel wind turbine (WT) model that can dynamically control reactive power is proposed based on the reactive power capability curve of a DFIG. Additionally, a modified operational cost form of wind power that accounts for wind power's volatility is explored.
- A new bi-level multi-objective strategy is used to solve the RPP problem considering the uncertain feature of loads and WTs. In the upper level, the MOGA is utilized to optimally assign new VAR sources and determine the best-connected WT locations. A modified fuzzy min-max technique is presented to find the optimum solution.

The remnant of the paper is arranged as follows: the uncertainty of wind power and load demand with WT modelling are discussed in Section 2. A multi-objective RRP problem formulation is described in Section 3. The proposed solution algorithm for solving the RPP is discussed in Section 4. Section 5 depicts the case study results and discussion. Finally, the conclusions are presented in Section 6.

2. Load and wind power uncertainty modelling

Many random factors occur in the power system; this section discusses the uncertainty of load demand and generated wind power.

2.1. Load demand uncertainty modelling

Electrical power systems' stochastic loads necessitate modeling of demand uncertainty at the planning and operation stages. The normal Gaussian PDF [17] can be used to describe load uncertainty in general. Fig. 1 shows the load levels and probability of each d_{th} load scenario which represented by $f(P_D)$ and calculated as [14]:

$$f(P_D) = \int_{P_D^{min}}^{P_D^{max}} \frac{1}{\sqrt{2\pi\sigma^2}} e^{-\frac{(P_D-\mu_D)^2}{2\sigma^2}} dP_D \tag{1}$$

where, $f(P_D)$ is the probability of the d_{th} load scenario, $P_{D_d}^{max}$ and $P_{D_d}^{min}$ are the boundaries of d_{th} load scenario, and μ_D and σ are the mean and variance of the load scenario, respectively.

2.2. Wind power uncertainty modelling

Wind power generation is dependent on the farm's location and fluctuates over time owing to changes in wind speed. Since wind speed is a random variable, the uncertainty must be represented in the output power of the wind generators. Weibull distributions [26] are a widely used model for wind speed. The wind speed's Weibull PDF is shown in Fig. 2(a) and is computed as [1]:

$$PDF(U) = \left(\frac{k}{C}\right)\left(\frac{U}{C}\right)^{k-1} e^{-\left(\frac{U}{C}\right)^{k}} \tag{2}$$

where U is the wind speed, k is the shape parameter and C is the scale parameter. The probability of certain ranges of wind speed in each scenario can be obtained as [1]:

$$f(U) = 1 - e^{-\left(\frac{U}{C}\right)^{k}} \tag{3}$$

The relationship between the WT 's active output power P_w and the wind speed U shown in Fig. 2(b) and can be approximated as [27]:

$$P_w = \begin{cases} 0 & 0 \le U \le U_{ci} \\ P_{rw}\dfrac{U-U_{ci}}{U_r-U_{co}} & U_{ci} \le U \le U_r \\ P_{rw} & U_r \le U \le U_{co} \\ 0 & U_{co} \le U \end{cases} \tag{4}$$

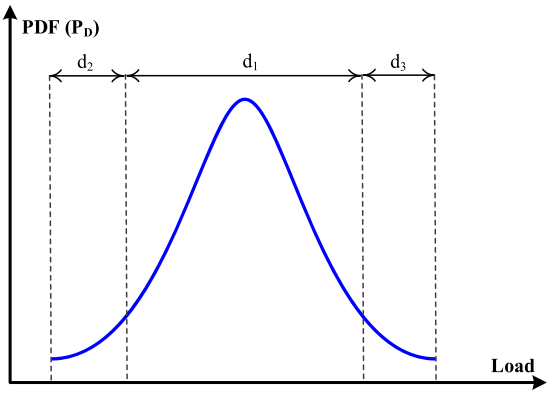

Fig. 1. Load characterization PDF.

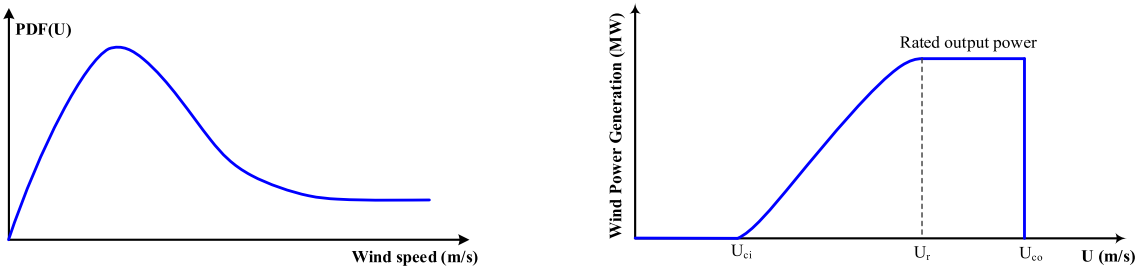

(a) Wind speed characterization PDF (b) WT power curve

Fig. 2. WT Performance, (a) Wind speed characterization PDF,(b) WT power curve.

where, P_{rw} represents the rated output power of the WT, and U_{ci}, U_r and U_{co} represent the cut-in wind speed, rated wind speed, and cut-out wind speed, respectively.

It indicates that no net power is generated below the cut-in wind speed. The produced wind power rises as the wind speed increases. Once the rated wind speed is reached, the WT operates at rated power. That is, when the wind speed is between the rated and cut-out wind speeds, the output equals the generator's rated power. Because the wind is too powerful to operate safely above the cut-out wind speed, the WT must be forced to shut down, and the output power is reduced to zero.

2.3. Modeling of WT

The two types of WTs are fixed-speed and variable-speed, with the DFIGs being one of the most common types of variable-speed generators used in WT units [17]. Fig. 3 depicts the basic structure of DFIG-based WTs. The stator of this machine is directly connected to the power grid, while the rotor is connected to the grid via an AC/DC/AC variable frequency power electronic converter. By changing the voltage magnitude and frequency, these converters can regulate the reactive power output of the wind generator. Because of the grid-side converters, DFIG may be able to provide dynamic reactive power regulation. As a result, the WT's reactive power injection could be used to its full potential. This overcomes the major shortcoming of previous methods in terms of available reactive power, which is restricted either to a fixed regulation band or to a maximum power factor. The power converter also allows the DFIG machine to be regulated between sub-synchronous and super-synchronous speeds (greater than synchronous speed), with a typical range of -40 to +30% [17].

The total injected reactive power into the grid by wind generators (Q_w) is made up of the sum of the injected reactive power by the DFIG stator (Q_s) and the reactive power injected by the DFIG grid side converters (Q_{gsc}).

$$Q_w = Q_s + Q_{gsc} \tag{5}$$

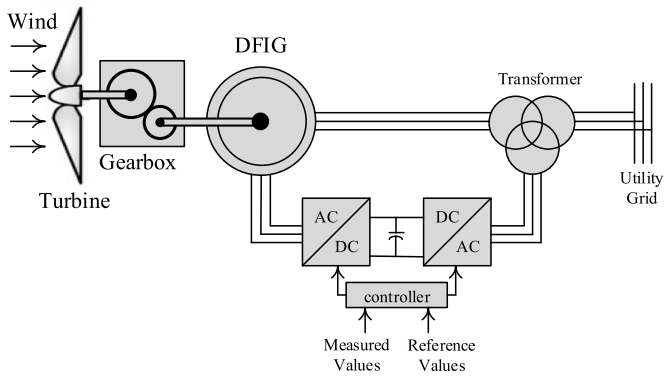

Fig. 3. DFIG structure.

The reactive power from the generator stator side may be determined as [28]:

$$Q_s = 3I_s\ V_s \sin\varnothing_s \tag{6}$$

where, I_s and V_s is the stator current and voltage, respectively, and $\varnothing_s$ is the phase angle between the stator voltage and current.

The reactive power capability of DFIG grid side converters can be given as follows [28]:

$$Q_{gsc} = \pm\sqrt{S_{gsc}^2 - P_{rw}^2} \tag{7}$$

where, S_{gsc} is the MVA capacity of the grid side converter.

The maximum limit of stator reactive power injection is restricted by the rated rotor current and the rated rotor voltage; however, while the machine is consuming reactive power, the stator current acts as the limit factor [28], as illustrated in Fig. 4.

3. Problem formulation

The aim of the present study is to solve the RPP issue in the presence of uncertain wind power and loads. Thus, the problem has been modelled as a multi-objective nonlinear optimization problem and solved in a bi-level structure. At the upper level, a MOGA is concerned with the optimum allocation of added new VAR sources where improving VS and minimizing the cost of new VAR sources are the objectives. At this level, the locations of added VAR sources (shunt/series) and the best connecting points of WT are initially determined by means of many factors. Then, a MOGA takes place to determine the appropriate value of each VAR source for different scenarios of load level and wind speed behaviors. The operational cost is minimized at a lower level by addressing an optimum power flow problem. A schematic diagram of

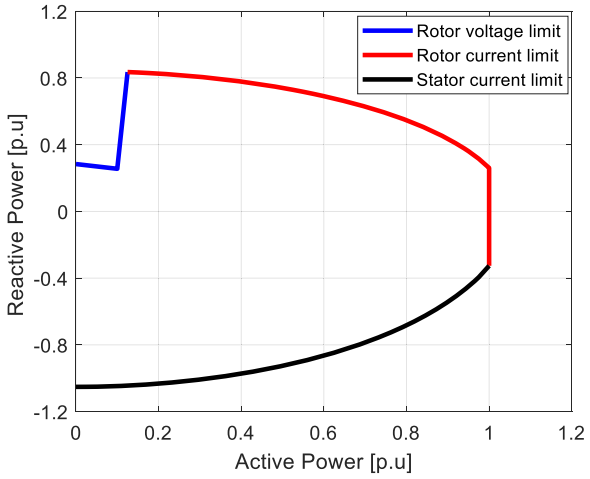

Fig. 4. DFIG-based WT dynamic reactive power capability.

how to solve the problem is shown in Fig. 5.

The new VAR sources should provide secure operation under any conditions. As a result, the upper level assumes three different load scenarios (light/base/peak) and two wind power levels (worst/best). This results in six scenarios, each with six different values for each of our VAR sources. The highest of these values is chosen as the final selected value for each source. This ensures the network's security to the fullest extent feasible under any operational condition. At the upper level, the goal is to improve voltage stability while minimizing the cost of new VAR sources. At the lower level, the total operating costs are reduced by adjusting a variety of control variables such as generator voltages and changing the transformer tap ratio, as well as optimizing the allocation of generated power and controlling the output (setting) value of the new VAR sources. The optimal setting of VAR sources is limited by their available sizing (which is obtained from the upper level).

3.1. Optimal location of VAR sources and WT

3.1.1. Optimal new VAR source location

3.1.1.1. Shunt sources. The L-index indicator is used to define the locations of the shunt reactive power compensation source. It is based on load flow analysis and its value ranges from zero when there is no load to one when there is voltage collapse. Because the bus with the greatest L–index value is the system's weakest bus, these buses are chosen and ranked as a suitable site for a new VAR source. The following is a discussion of the L–index calculation [27]:

$$\begin{vmatrix} I_G \\ I_L \end{vmatrix} = \begin{vmatrix} Y_{GG} & Y_{GL} \\ Y_{LG} & Y_{LL} \end{vmatrix} \begin{vmatrix} V_G \\ V_L \end{vmatrix} \tag{8}$$

whereI_G, I_L, V_G and V_L are the currents and voltages at generator and load buses and Y is the admittance matrix. Rearranging (8) we get:

$$\begin{vmatrix} V_L \\ I_G \end{vmatrix} = \begin{vmatrix} Z_{LL} & F_{LG} \\ K_{GL} & Y_{GG} \end{vmatrix} \begin{vmatrix} I_L \\ V_G \end{vmatrix} \tag{9}$$

where,

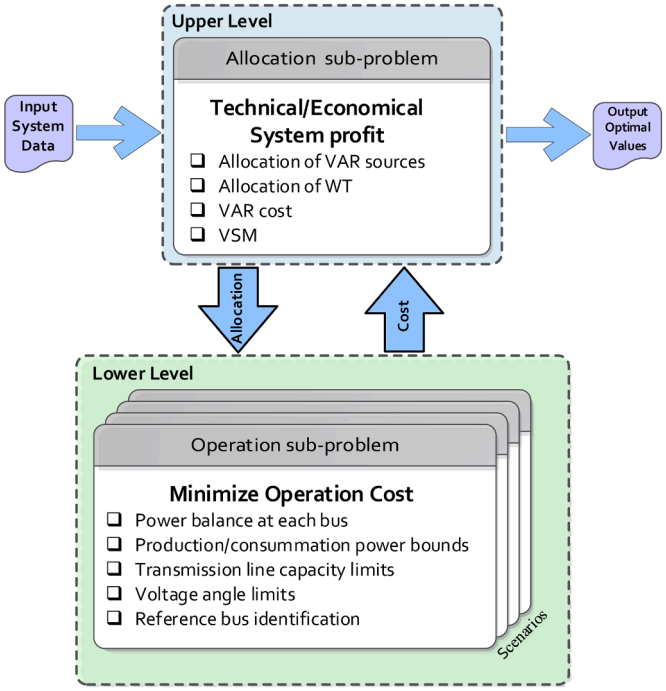

Fig. 5. Schematic diagram for the proposed bi-level solution method.

$$F_{LG} = -|Y_{LL}|^{-1}|Y_{LG}| \tag{10}$$

The L-index of bus j is given as:

$$L_j = \left| 1 - \sum_{i=1}^{N_g} F_{ji} \frac{V_i}{V_j} \angle(\theta_{ji} + \delta_{ij}) \right| \tag{11}$$

where F_{ji} is the elements in the matrix F_{LG}, and θ_{ji} is the phase angle of the term F_{ji}.

3.1.1.2. Series sources. The series reactive power compensation sources are located at the most critical lines which are defined by the fast voltage stability index (FVSI) [29]. It is built on the idea of power flowing through a single line. The FVSI is computed for a typical transmission line by [29]:

$$FVSI_{ij} = \frac{4Z_{ij}^2 Q_j}{V_i^2 X_{ij}} \tag{12}$$

where, Q_j is the receiving end total reactive power flow. The line with an index value that is closer to 1 is the most crucial line for series compensation in the system, because it may cause the entire system to become unstable and is chosen as a suitable location.

3.1.2. Optimal WF location

The optimal connection points of available buses in different regions where WT might be installed are selected to reduce the line congestion. Based on the power transfer distribution factors (PTDFs), the connecting points may be identified. It may be defined as the line flows sensitivity to changes in nodal active power injection. It is the ratio of power flow changes on line l (between buses i and j) as a result of the power transaction from the bus m to n. The most positive amounts of PTDFs mean that at the related buses any generation increase (or any load decrease) results in a reduction in line congestion [30].

$$PTDF_l = \frac{\Delta P_l}{\Delta P_{bus}} = \left(X_{im} - X_{jm} - X_{in} + X_{jn}\right) \Big/ X_{ij} \tag{13}$$

where, X_{im} is the element of the bus reactance matrix in the i^{th} row and m^{th} column.

3.2. The objective functions

3.2.1. Minimization of VAR investment cost

The first goal is to minimize the investment costs of new VAR sources (IC_{VAR}) which are calculated as follows:

$$IC_{VAR} = \sum_{i \in N_{cap}} C_{Cap.i} + \sum_{l \in N_{TCSC}} C_{TCSC.l} \times S_{TCSC.l} + \sum_{i \in N_{SVC}} C_{svc.i} \times Q_{svc.i} \tag{14}$$

The objective function in (14) consists of three parts represent the installation costs of the capacitor banks, TCSC, and SVC respectively, where [24];

$$C_{Cap,i} = C_F + C_c \, Q_{c,i} \tag{15}$$

$$C_{TCSC,l} = 0.0015 S_{TCSCl}^2 - 0.7131 S_{TCSC.l} + 153.57 \tag{16}$$

$$C_{svc,i} = 0.0003 Q_{SVC,i}^2 - 0.3051 Q_{svc.i} + 127.38 \tag{17}$$

In this study, C_c=3 × 10^4\$/MVAR and C_F=1000\$ [31]. The total VAR device annual installing cost is given by [24]:

$$AIC_{VAR} = IC_{VAR} \frac{ir\,(1+ir)^{LT}}{(1+ir)^{LT} - 1} \tag{18}$$

The LT is supposed to be 10 years, and *ir* to be 10%

3.2.2. Improving the voltage stability

Voltage stability is "the ability of a power system to maintain acceptable voltages at all buses under normal conditions and after being subjected to a disturbance" [32]. The failure of power systems to satisfy the demand for reactive power is the principal factor causing voltage instability. The relation between power and voltage (P-V or MW margins) is used in power systems to assess a system's ability to sustain VS under regular and abnormal conditions [33]. The P-V relation is obtained through a series of solutions for AC power flow. As a consequence of increased power transfer between two nodes in the system, there is a reflection of voltage shifts, Fig. 6 shows the relation between power loading and system voltage. The distance between the base case loading and the loading that leads to voltage collapse is called the VS margin (VSM), which can be measured in p.u. as follows [34]:

$$VSM = (P_{D.max} - P_D)/P_D \tag{19}$$

The aim of this study is to RPP problem in the power system, not only for the purpose of improving the bus voltage but also to increase the VSM and thus increase the ability of the system to face any emergency.

3.2.3. Minimization of operating cost

The operating cost is minimized at the lower level by running optimal power flow. This is accomplished by controlling a number of decision variables like updating the tap ratio of transformers, controlling the active and reactive output of conventional generators, selecting scheduled active power from each WF, controlling WF reactive power output according to its minimum and maximum limits at this scheduled value based on Fig. 4, and changing the output MVAR from the added VAR sources based on their approved limits from the upper-level results. The total operation cost (C_{PG}) of generated power can be formulated as:

$$C_{PG} = \sum_{i=1}^{N_s} C_i(P_g)\, f_i(P_D)\ i = 1, 2, \ldots N_s \tag{20}$$

where $C_i(P_g)$ is the operation cost of generated power for the load scenario i^{th}, and $f_i(P_D)$ is the probability of the i^{th} load scenario. This operation cost is divided into two components as follows:

$$C_i(P_g) = C_{gi}(P_{gi}) + C_{wi}(P_{wi}) \tag{21}$$

where $C_{gi}(P_{gi})$, and $C_{wi}(P_{wi})$ are the operation cost of the thermal generators and WF, respectively. The operation cost of the thermal generators with quadratic cost functions is formulated as follows [35]:

$$C_{gi}(P_{gi}) = \sum_{i=1}^{N_g} a_i (P_{gi})^2 + b_i\, P_{gi} + c_i \tag{22}$$

where a_i, b_i, and c_i are the i^{th} thermal generator cost coefficients.

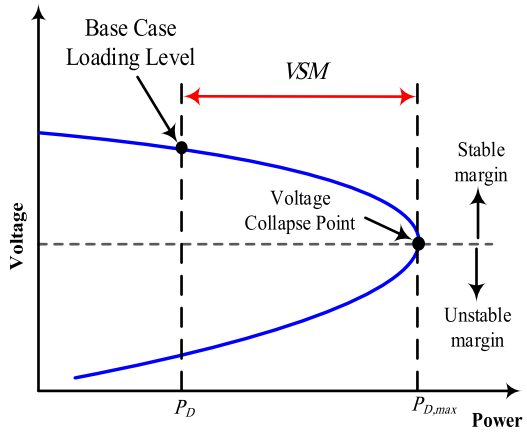

Fig. 6. The relation between power loading and bus voltage.

The problem of wind power cost is examined from a new perspective in this study, as the operating cost of wind power is estimated by combining three mathematical components and can be expressed as [35]:

$$C_{wi}(P_{wi}) = C_{h_{wi}}\, P_{wi} + C_{P_{wi}}\,(P_{w_{avi}} - P_{wi}) + C_{r_{wi}}\,(P_{wi} - P_{w_{avi}}),\ i = 1, 2, 3, \ldots, N_w \tag{23}$$

where $C_{h_{wi}}$ is operation cost of the i^{th} WF per MW. $C_{P_{wi}}$ and $C_{r_{wi}}$ are the imbalance cost of i^{th} WF due to underestimation and overestimation of the scheduled wind power respectively. $P_{w_{avi}}$ and P_{wi} are the available and scheduled wind power from i^{th} WF respectively.

The first term in (23) is the cost of actual generated or scheduled wind power. The penalty for underestimating and overestimating wind power output is addressed in the final two terms of (23). The scheduled wind power cannot always equal the available wind power because it is a stochastic variable. As a result, underestimation and overestimation costs must be included in the objective function. The cost of underestimating wind power is considered to be linearly related to the integral of the product of the PDF of wind power and the discrepancy between available and scheduled wind power. The functional meaning of this concept is related to the penalty of wind energy curtailment:

$$C_{P_{wi}}\,(P_{w_{avi}} - P_{wi}) = C_{P_{wi}} \int_{P_{wi}}^{P_{rw}} (w - P_{wi}) f(P_w)\, dw \tag{24}$$

where, $f(P_w)$ is the Weibull PDF of i^{th}WF output power and w is the integral variable.

Similarly, the overestimation penalty cost is calculated. The required reserve cost for a wind power deficit is the functional meaning of this concept, which may be stated as follows:

$$C_{r_{wi}}\,(P_{wi} - P_{w_{avi}}) = C_{r_{wi}} \int_{0}^{P_{wi}} (P_{wi} - w) f(P_w)\, dw \tag{25}$$

So, the total cost (TCO) is the sum of the new VAR sources cost and the total operating cost and can be expressed by:

$$TCO = C_{PG} + AIC_{VAR} \tag{26}$$

3.3. Problem constraints

Many constraints must be fulfilled to ensure that the system is capable to operate in a stable and reliable state. Also, these system constraints assure the desired solution achieved is acceptable for the functional operation of the power system.

- Active and reactive power balance:

$$P_{gi} - P_{Di} - V_i \sum_{j=1}^{N_b} V_j \left(G_{ij}\cos\delta_{ij} + B_{ij}\sin\delta_{ij}\right) = 0,\ i \in N_b \tag{27}$$

$$Q_{gi} - Q_{Di} + Q_{ci} + Q_{ci}^{o} - V_i \sum_{i=1}^{N_b} V_j \left(G_{ij}\sin\delta_{ij} - B_{ij}\cos\delta_{ij}\right) = 0,\ i \in N_b \tag{28}$$

- Buses voltage limits:

$$V_i^{min} \le V_i \le V_i^{max},\ i \in N_b \tag{29}$$

- Thermal generator active and reactive power limit:

$$\begin{cases} Q_{Gi}^{min} \le Q_{gi} \le Q_{Gi}^{max} \\ P_{Gi}^{min} \le P_{gi} \le P_{Gi}^{max} \end{cases},\ i \in N_g \tag{30}$$

- Transmission line flow limit:

$$|S_l| \le S_l^{max},\ l \in N_L \tag{31}$$

- Transformer tap setting limit:

$$T_K^{min} \le T_K \le T_K^{max},\ k \in N_T \tag{32}$$

- Wind active and reactive power limits:

$$\begin{cases} 0 \le P_{wi} \le P_{rw} \\ Q_{Wi}^{min} \le Q_{wi} \le Q_{Wi}^{max} \end{cases},\ i \in N_w \tag{33}$$

- New VAR source limits:

$$\begin{cases} Q_{ci}^{min} \le Q_{ci} \le Q_{ci}^{max},\ i \in N_{cap} \\ Q_{SVCi}^{MIN} \le Q_{SVCi} \le Q_{SVCi}^{max},\ i \in N_{SVC} \\ -0.8X_{ij} \le X_{TCSCi} \le 0.2X_{ij},\ i \in N_{TCSC} \end{cases} \tag{34}$$

4. Proposed solution algorithm

Because the RPP objective functions and constraints are complicated, non-smooth, and non-differentiable, the conventional methods fail to adequately address this issue. MOGA as an evolutionary algorithm is employed to overcome the drawbacks of conventional methods. The GA is interested in natural genetics and natural selection search mechanisms [11,36]. The multi-objective optimization problem can be formulated as:

Maximizing, Minimizing $f_i(x,u),\ i = 1, 2, 3, \ldots\ldots N_{obj}$

Subject to $g(x,u) = 0$ Equality constraints

$h(x,u) \le 0$ Inequality constraints where, $f_i(x,u)$ is the objective function, u is the state variables set, and x is the controllable variable set. It can simply be seen as an attempt to find the best possible solution for the objective function using a collection of controllable variables. In this study, MOGA is employed with a number of competing aims and restrictions.

Two general approaches are utilized to address multiple-objective optimization problems. In the first technique, the individual objective functions with weighted factors are combined into a single composite function. The second method used in this work is to directly search for the complete Pareto optimum set. The notion of an ideal optimization approach for multiple objectives is to describe several optimum trade-off solutions with a wide range of objective function values, and then pick one of the solutions based on the system operator's requirements.

Using a fuzzy min-max approach, the optimal compromise solution can be calculated. The i^{th} objective function F_i is expressed using the fuzzy membership function λ_i, and is expressed as:

$$\lambda_i = \begin{cases} 1 \text{ if } f_i \le F_i^{min} \\ \dfrac{F_i^{max} - f_i}{F_i^{max} - F_i^{min}} \text{ if } F_i^{min} < f_i < F_i^{max} \\ 0 \text{ if } f_i \ge F_i^{min} \end{cases} \tag{35}$$

where, F_i^{min} and F_i^{max} are the minimum and maximum values of the i^{th} objective function among all non-dominated solutions, respectively.

Although the previous equation is appropriate when minimizing the cost is the objective function, but it is found that not appropriate when the objective function is to improve the system VS. So, A noticeable change has happened in the normalization of the second objective function since this objective aimed to be maximized during the optimization procedure, and is expressed as:

$$\lambda_i = \begin{cases} 1 \text{ if } f_i \le F_i^{min} \\ \dfrac{f_i - F_i^{min}}{F_i^{max} - F_i^{min}} \text{ if } F_i^{min} < f_i < F_i^{max} \\ 0 \text{ if } f_i \ge F_i^{min} \end{cases} \tag{36}$$

The normalized membership function (λ^c) for each non-dominated solution M, is determined using:

$$\lambda^c = \frac{\sum_{i=1}^{N_{obj}} \lambda_i}{\sum_{c=1}^{M} \sum_{i=1}^{N_{obj}} \lambda_i} \tag{37}$$

The best compromise solution is the one with the highest λ^c value. The steps of the proposed RPP solution algorithm are as follows:

Step 1: Read the network data (generator, branch, bus, etc.…).

Step 2: Determine the optimal location of the new VAR source and the connection points of WFs using L-index, FVSI, and PTDF.

Step 3: Read the load scenarios.

Step 4: Read the wind scenarios.

Step 5: Select the parameters of MOGA: generations number, population size, etc.….

Step 6: Set the generation count and initialize randomly the population.

Step 7: Identify the boundary limits of the control variables and define the limits of VAR sources values share it to the lower level.

Step 7: Update network data based on RPP solving technique and then run power flow.

Step 8: Examine the objective functions (VSM & total cost) and verify the system constraints.

Step 9: Implement the GA process; mutation, selection, and crossover then update the population for the next generation.

Step 10: Repeat the steps from 7 to 9 where the generation count is increased till the stopping criteria are satisfied or the number of generations reaches its maximum value.

Step 11: Apply the fuzzy min-max approach and select the optimal solution for this scenario from the Pareto solutions.

Step 12: Update the wind scenario and repeat the steps from 5 to 11 until the last scenario.

Step 13: Update the load scenario and repeat the steps from 4 to 12 until the last scenario.

Step 14: Select the final approved value of each VAR source from all scenarios.

Fig. 7 depicts the flowchart for the proposed algorithm.

5. Case study and results

To evaluate the effectiveness of the suggested MOGA-based approach to solving the RPP problem, it is applied to the updated IEEE 30-bus test system and a part of the electricity grid in South Egypt.

5.1. Modified IEEE 30-bus system

The modified IEEE 30-bus test system is shown in Fig. 8, and the network data are taken from [37]. This system includes 6 generators, 41 transmission lines, and 24 load buses, of which four branches (4–12), (6–9), (6–10), and (28–27) are with the tap changing transformer. The lower and upper limits for voltage magnitude of the load buses are 0.95 p.u. and 1.05 p.u. The transformer tapping is changed between 0.9 and 1.1 p.u. with the step size 0.025.

The network will be supported by eight new VAR sources, which satisfy the maximum system loadability [38]. These VAR sources may be either capacitor banks, FACTS, or a mixture of them. The new capacitor banks have a rating between 0 to 5 MVAR with a step size of 1 MVAR. Three WFs will be allocated by the MOGA in three areas with a greater abundance of wind energy, each of which has limited potential network

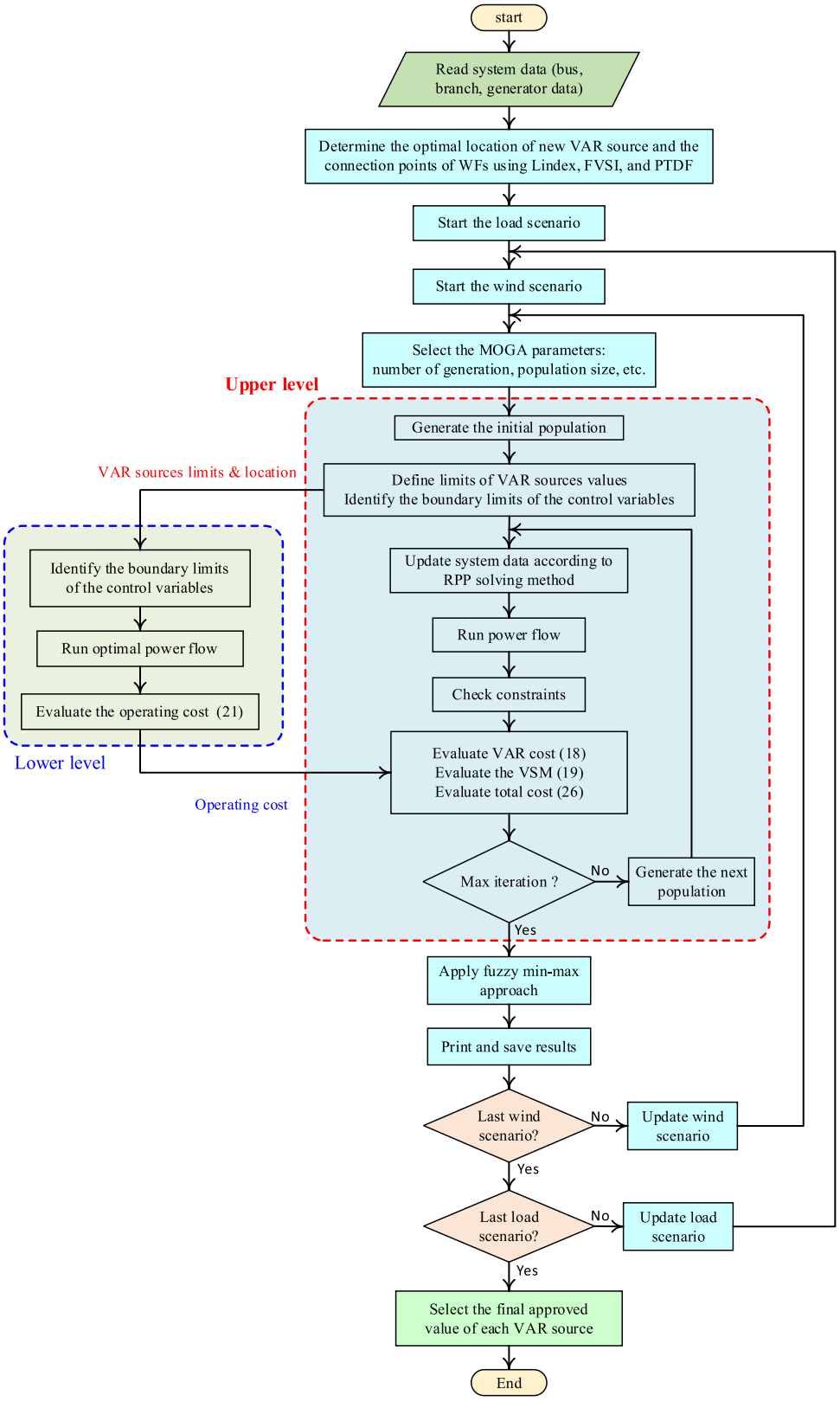

Fig. 7. The proposed flowchart algorithm.

connection points. Table 2 shows the allowed installation capacity of the WFs and the possible connection points of each region. The wind power generation data is taken according to [28].

The normal Gaussian PDF and Weibull PDF are used for modeling the load and wind speed uncertainties, respectively. Three scenarios for loads are modeled which represent different levels of loads (light, base, and peak). The features of these different scenarios are summarized in Table 3.

Many buses have voltages that are beyond the limit before installing WFs and new VAR sources. The voltage at the system buses is shown in

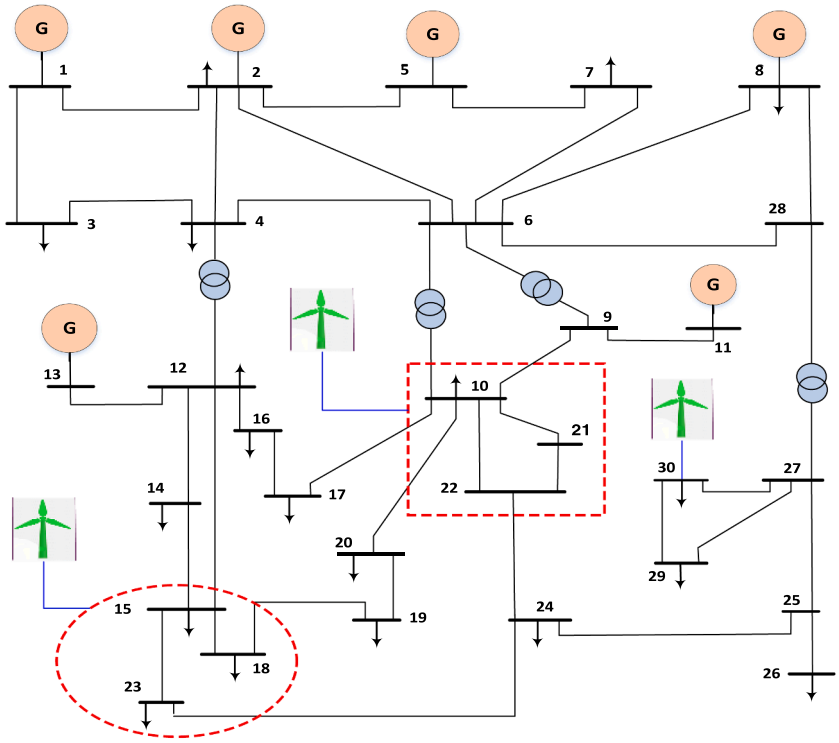

Fig. 8. Modified IEEE 30 bus single line diagram.

Table 2
WF capacity and suggested location for different regions.

Item	Allowed capacity [MW]	Available connecting points
WF1	20	Bus no. 15, 18, 23
WF2	16	Bus no. 10, 21, 22
WF3	26	Bus no. 30

Table 3
Load scenarios.

Load interval	Load%	PDF_d
d_1	65	0.15
d_2	85	0.7
d_3	105	0.15

Fig. 9, and it is obvious that the minimum voltage of 0.898 p.u. occurs at bus 30. As a result, there is an urgent need to supplement the network with more VAR resources.

Buses 18, 21, and 30 are appropriate connection points for WFs employing the PTDF for the first, second, and third WFs, respectively. The appropriate buses for shunt VAR sources are 30, 29, 26, 25, 27, 24, 23, and 19. FVSI's series VAR sources are line 36 (28–27), line 12 (6–10), line 38 (27–30), and line 13. (9–11). The proposed approach is applied to the system under investigation to allocate the additional VAR sources optimally. Table 4 shows the optimal setting of VAR sources at each load-wind scenario for the three cases of VAR source type.

It is evident that there are six different values for each VAR source for the six supposed scenarios. For example, in the case of capacitors and assuming the (first/worst) scenario (peak load & zero wind speed) and by applying MOGA, there is a value for each VAR source, which is of course sufficient to meet the requirements in this scenario. The same goes for the rest of the scenarios. Then for VAR source No. 1, there are six values (3, 4, 3, 3, 2, 0, 0, and 0) MVAR one for each scenario. The final

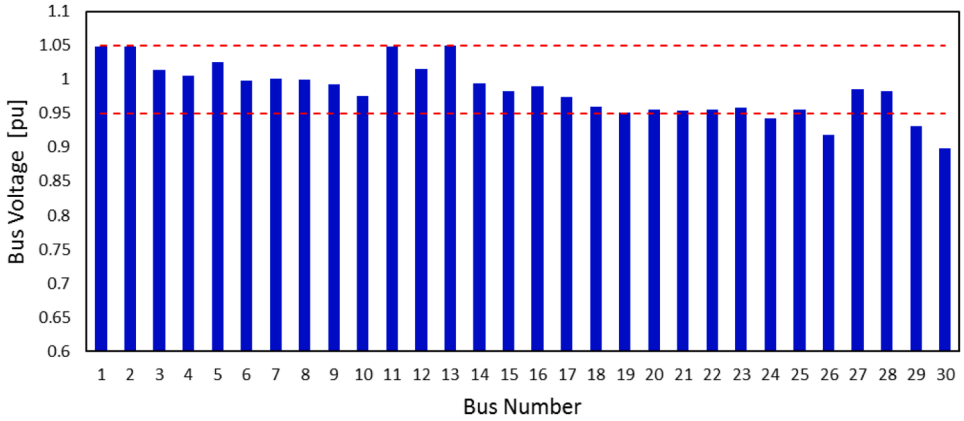

Fig. 9. Buses voltage pre-adding of new VAR devices.

Table 4
Optimal allocation of VAR sources under load-wind scenarios.

VAR Source Type		Location	VAR Size for peak load		VAR Size for base load		VAR Size for light load	
			Zero wind speed	Full wind speed	Zero wind speed	Full wind speed	Zero wind speed	Full wind speed
Capacitor Banks		Bus 30	3	1	5	1	5	5
		Bus 29	4	1	4	1	5	2
		Bus 26	3	1	3	1	4	4
		Bus 25	3	1	4	0	3	2
		Bus 27	2	2	3	1	5	3
		Bus 24	0	1	1	1	0	1
		Bus 23	0	2	0	0	0	0
		Bus 19	0	1	0	1	0	0
FACTS Devices	SVC 1	Bus 30	4.7	8.46	17.12	5.87	18.93	6.92
	SVC 2	Bus 29	1.14	9.89	5.47	3.52	6.96	14.62
	SVC 3	Bus 26	4.41	6.89	3.19	4.73	2.8	10.67
	SVC 4	Bus 25	4.31	6.94	7.16	2.27	2.31	19.65
	TCSC 1	Line 36	0.418	0.1176	0.3511	0.351	0.2942	0.4027
	TCSC 2	Line 12	0.3137	0.2635	0.3161	0.3072	0.3151	0.3122
	TCSC 3	Line 38	0.4721	0.3479	0.4135	0.2712	0.0401	0.2438
	TCSC 4	Line 13	0.1583	0.021	0.0348	0.155	0.0163	0.1592
Hybrid	SVC 1	Bus 30	1.43	3.71	4.08	2.19	10.54	3.91
	SVC 2	Bus 29	3.8	0.67	5.97	1.71	9.12	3.53
	Cap. 1	Bus 26	4	4	3	5	3	4
	Cap. 2	Bus 25	3	2	4	3	3	4
	Cap. 3	Bus 27	3	2	3	3	3	3
	TCSC 1	Line 36	0.3153	0.3159	0.3134	0.3132	0.3149	0.3086
	TCSC 2	Line 12	0.4022	0.4401	0.3504	0.4427	0.228	0.4343
	TCSC 3	Line 38	0.4689	0.4459	0.4122	0.3811	0.0686	0.2714

optimal selected solution -which is shown later is the largest value of 4 MVAR. It is worth noting that these values represent the size of the capacitors required, while the settings differ according to the operating condition.

The final selected VAR source locations and sizing are shown in Table 5 for each case (only capacitors, only FACTS, and hybrid cases). The final selected values are the largest values of VAR sources obtained in Table 4 for the six situations (load-wind scenarios). This ensures that the final setting of these sources is sufficient to compensate for reactive power shortage under different operational conditions, such as load or wind speed. It should be noted that the value of both capacitors and SVC is indicated in MVAR, while the TCSC is indicated in p.u.

The relation of VAR source cost and VSM for the case of using capacitors bank only at base load scenario is shown in Fig. 10. The figure clearly shows that the relationship is direct between the cost of the new capacitors and the increase of system VSM. Figs. 11 and 12 depict this relationship for the situation of employing FACTS devices and a hybrid assortment at the base load scenario. It turns out that the more we want to have a more stable system, the greater the expenditure required

Table 6 illustrates the total operating cost, which is the sum of fuel cost and wind power cost for the three cases of VAR types. Also, the VAR cost in each case and the value of VSM are presented. It has been shown that using the capacitor bank solely, for the purpose of achieving the maximum possible net savings, is more acceptable. However, it is no better way to improve the system VS. While the use of FACTS devices is the most effective in terms of enhancing the system VS, however, it comes at an expensive cost. It also demonstrates that using a hybrid of FACTS devices and capacitor banks as a combination to increase network VS yields good results at a medium cost. It is evident that the total operating cost was not significantly affected in the three different cases. While the total cost differs due to the variation in the cost of the new VAR sources in the three cases.

Table 7 compares the operational costs before and after the WFs are installed. It has been demonstrated that the installation of WFs has significantly reduced operational costs. It also resulted in a cost decrease for the needed VAR sources, and given the extent of the system's VS, where the value of the VSM increased, thereby improving the system's VS. This, of course, comes after the installation of new VAR sources. Renewable energy has significantly reduced total costs, not to mention its outstanding benefits in improving environmental conditions and emissions

The updated IEEE 30-bus test network performance is evaluated under different contingency states. Table 8 depicts the results of the simulation when the optimization algorithm is applied for line outage contingencies. The present work has proven its effectiveness in facing contingencies of multiple line outages in the network.

When the methodologies used to model wind power in the literature are studied, it is discovered that the reactive power output of a WF is represented either as a fixed band [3,6], or based on the constant power factor [1,10,11], or in a dynamic reactive power management way [17, 18]. However, it should be noted that in both references [17] and [18], the rotor voltage constraints in the wind power capability curve were neglected. Furthermore, because reactive power is represented as a fixed band, this clearly does not make the best use of the WF. A comparison of the results of the other two methods is presented in Table 9. The method used in this work makes better use of the WF reactive power capabilities, lowering the cost of the required new VAR sources. In addition, as seen in the previous table, the method adopted in this work produced superior results in terms of range system VS.

Table 5
Optimal VAR allocation for the three cases.

Item	Capacitors case	FACTS case	Hybrid case
VAR 1	5 @bus 30	19 @bus 30	11 @bus 30 SVC
VAR 2	5 @bus 29	15 @bus 29	10 @bus 29 SVC
VAR 3	4 @bus 26	11 @bus 26	5 @bus 26 Cap.
VAR 4	4 @bus 25	20 @bus 25	4 @bus 25 Cap.
VAR 5	5 @bus 27	0.418 @line 12	3 @bus 27 Cap.
VAR 6	1 @bus 24	0.3161 @line 36	0.3159 @line 36
VAR 7	2 @bus 23	0.4721 @line 38	0.4427 @line 12
VAR 8	1 @bus 19	0.1592 @line 13	0.4689 @line 38

5.2. South Egypt electricity network

A transmission network at 220 kV of the South Egypt network [39] is utilised to evaluate the proposed technique. Fig. 13 presents a single-line diagram of this network. The South Egypt power network is heavily loaded with a demand of 4778.5 MW and 2801.8 MVAR. Before adding new VAR sources, several buses' voltages are out of the limit where the Oyanat bus has a minimum voltage of 0.665 p.u. The newly configured

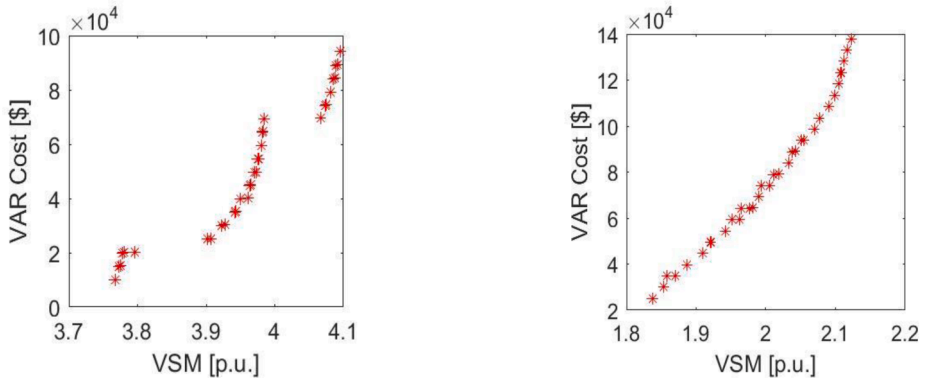

(a) Full wind speed scenario (b) Zero wind speed scenario

Fig. 10. Relation between VAR cost and VSM in the case of the capacitors for base load scenario. (a) Full wind speed scenario, (b) Zero wind speed scenario.

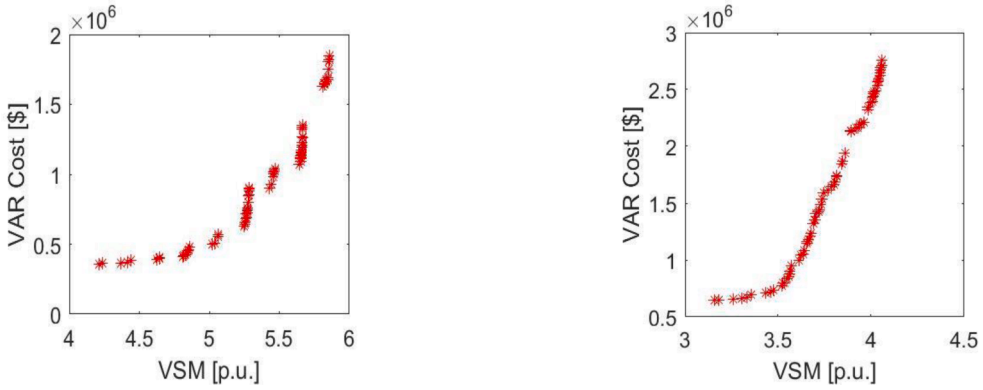

(a) Full wind speed scenario (b) Zero wind speed scenario

Fig. 11. Relation between VAR cost and VSM in the case of the FACTS for base load scenario. (a) Full wind speed scenario, (b) Zero wind speed scenario.

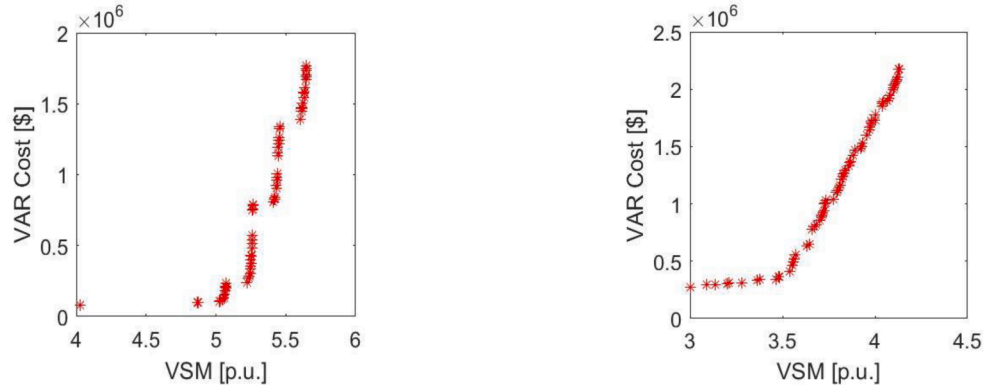

(a) Full wind speed scenario (b) Zero wind speed scenario

Fig. 12. Relation between VAR cost and VSM in the case of the Hybrid for base load scenario. (a) Full wind speed scenario, (b) Zero wind speed scenario.

Table 6
The operating cost for different new VAR cases.

Item	Capacitor's case	FACTS case	Hybrid case
VAR cost [$]	1.33×10^5	14.5×10^5	9.12×10^5
Wind cost [$]	1.296×10^6	1.26×10^6	1.26×10^6
fuel cost [$]	5.8×10^6	6.15×10^6	6.15×10^6
Total operating cost [$]	7.096×10^6	7.41×10^6	7.41×10^6
Total cost [$]	7.229×10^6	8.86×10^6	8.322×10^6
VSM [p.u.]	3.34	4.46	4.44

Table 7
The effect of installing WFs in the case of using a capacitor bank.

Item	Without WFs	With WFs
operating cost [$]	1.02×10^7	7.096×10^6
VAR cost [$]	1.97×10^5	1.33×10^5
Total cost [$]	10.397×10^6	7.229×10^6
VSM [p.u.]	1.65	3.34

Table 8
The optimization algorithm results in line outage contingencies in the IEEE 30-bus system.

Outage line number*	From bus	To bus	Operating cost × 10^6 [$]	VSM [p.u.]	Outage line number*	From bus	To bus	Operating cost × 10^6 [$]	VSM [p.u.]
1	1	2	7.81	4.06	21	16	17	7.74	3.70
2	1	3	7.78	3.93	24	19	20	7.75	3.91
3	2	4	7.77	3.94	26	10	17	7.76	4.10
4	3	4	7.77	3.93	27	10	21	7.75	3.4
5	2	5	7.91	3.84	28	10	22	7.77	3.92
6	2	6	7.77	3.95	29	21	22	7.75	3.90
7	4	6	7.77	4.06	30	15	23	7.74	3.07
8	5	7	7.77	3.93	31	22	24	7.76	3.28
9	6	7	7.81	4.10	32	23	24	7.76	3.72
10	6	8	7.77	3.70	33	24	25	7.75	3.75
17	12	14	7.74	3.66	37	27	29	7.76	3.32
18	12	15	7.75	3.57	39	29	30	7.75	3.70
19	12	16	7.77	3.88	40	8	28	7.77	3.86
20	14	15	7.75	3.87	41	6	28	7.77	3.76

*The lines that lead directly to disconnection of a load or generator were not taken into account, as well as the lines on which transformers or TCSC are supposed to be installed.

Table 9
A comparison results between the suggested technique and those reported in the literature.

Item		Capacitor case	FACTS case	Hybrid case
Present work	VAR cost [$]	1.33 × 10^5	14.5 × 10^5	9.12 × 10^5
	VSM [p. u.]	3.34	4.46	4.44
Refs. [1, 10, 11] and [14]*	VAR cost [$]	1.477 × 10^5	21.351 × 10^5	9.915 × 10^5
	VSM [p. u.]	3.31	4.45	4.35

*The power factor is ranged between 0.98 lag and 0.98 lead.

capacitance bank setting hit 80 MVAR as a result of the heavy system loading. The system is supported by three WFs with a capacity of 50, 125, and 125 MW at buses Faum, Sfaga, and Hurgda, respectively. Using the L-index factor shows that the weakest busses are Oyanat, Tshka2, Tshka1, Balat, Hurgda, Mdecow, Tartor, and Sfaga. The weakest lines by FVSI are the lines between (Tshka1-Oynat), (A.Dam-Tshka1), (A.Dam--Mdecow), and (Nag.Ha-Tartor).

In table 10, the value of each VAR source is cleared in two scenarios of zero and rated output power of WTs at base load. Table 11 shows the final optimal approved value of each VAR source which is the maximum value in the two scenarios.

Table 12 shows the overall cost in each of the three cases. As the results show, any FACTS, capacitor bank, or a hybrid of the two might compensate for the system's lack of reactive power. If the capacitor

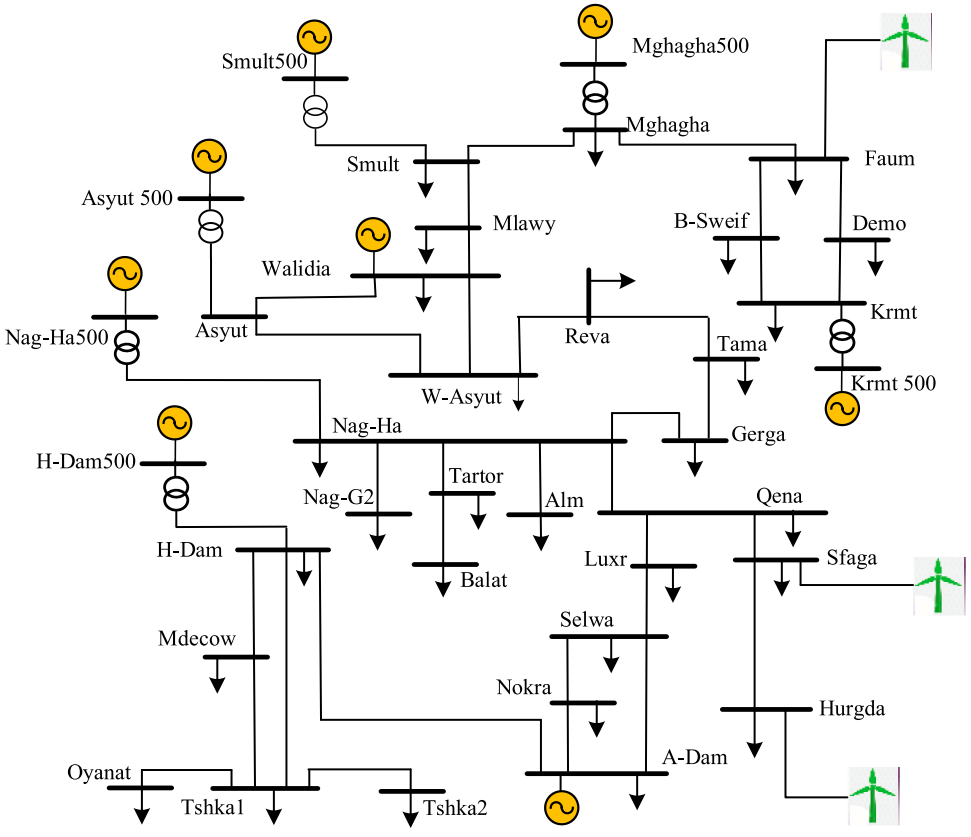

Fig. 13. South Egypt Electricity network.

Table 10
Optimal VAR sources values for each wind scenario for the three cases.

VAR sources	Capacitors case		FACTS case		Hybrid case	
	Zero wind speed	Full wind speed	Zero wind speed	Full wind speed	Zero wind speed	Full wind speed
VAR1	61	63	68 SVC	10 SVC	10 SVC	35 SVC
VAR2	71	75	72 SVC	16 SVC	52 SVC	30 SVC
VAR3	71	72	22 SVC	14 SVC	8 Cap.	7 Cap.
VAR4	4	4	18 SVC	14 SVC	15 Cap.	15 Cap.
VAR5	3	3	0.002 TCSC	0.1578 TCSC	7 Cap.	5 Cap.
VAR6	50	79	0.0681 TCSC	0.1058 TCSC	0.1548 TCSC	0.0687 TCSC
VAR7	6	4	0.0583 TCSC	0.0583 TCSC	0.0804 TCSC	0.1078 TCSC
VAR8	3	2	0.069 TCSC	0.0604 TCSC	0.0599 TCSC	0.0003 TCSC

Table 11
Final approved VAR sources values for the three cases.

Item	Capacitor case		FACTS case		Hybrid case	
	Value	location	value	location	value	location
VAR1	63	Oyanat	68 SVC	Oyanat	35 SVC	Oyanat
VAR2	75	Tshka2	72 SVC	Tshka2	52 SVC	Tshka2
VAR3	72	Tshka1	22 SVC	Tshka1	8 Cap.	Tshka1
VAR4	4	Balat	18 SVC	Balat	15 Cap.	Balat
VAR5	3	Hurgda	0.1578 TCSC	Tshka1 - Oyanat	7 Cap.	Hurgda
VAR6	79	Mdecow	0.1058 TCSC	A.Dam - Tshka1	0.1548 TCSC	Tshka1 - Oyanat
VAR7	6	Tartor	0.0583 TCSC	A.Dam - Mdecow	0.1078 TCSC	A.Dam - Tshka1
VAR8	3	Sfaga	0.069 TCSC	Nag.Ha - Tartor	0.0599 TCSC	A.Dam - Mdecow

Table 12
The operating cost for different three cases.

Item		Capacitor's case	FACTS case	Hybrid case
Without WFs	VAR cost [$]	21.7×10^5	96.4×10^5	60.3×10^5
	fuel cost [$]	8.263×10^8	8.25×10^8	8.242×10^8
	Total cost [$]	8.2847×10^8	8.3464×10^8	8.3023×10^8
	VSM [p.u.]	1.274	1.854	1.726
With WFs	VAR cost [$]	1.4948×10^5	46.665×10^5	32.275×10^5
	Wind cost [$]	1.82×10^7	1.81×10^7	1.81×10^7
	fuel cost [$]	6.78×10^8	6.79×10^8	6.79×10^8
	Total operating cost [$]	6.962×10^8	6.971×10^8	6.971×10^8
	Total cost [$]	6.9635×10^6	7.0177×10^6	7.0033×10^6
	VSM [p.u.]	1.296	2.635	1.823

banks are simply utilised to compensate for the reactive power, the operation is less costly, but the VS indication does not raise to the desired level. However, using FACTS devices provide us with a more stable system, although it is, of course, more expensive than the previous one. Whereas using a combination of capacitors and FACTS allowed us to build a network with high stability at a reasonable middle cost. It also notes that great savings were caused by relying on of WFs in the system, as well as the increase in stability in light of the additional inauguration of new VAR sources as well.

6. Conclusions

A probabilistic multi-objective RPP framework for power systems with substantial wind energy penetration has been described. Based on the reactive power capability curve of DFIG, a novel WT model that can dynamically adjust reactive power is developed. A new bi-level optimization strategy that accounts for load and wind power uncertainty to solve the RPP problem has been proposed. A MOGA is utilized at the upper level to discover the best connecting positions of WFs and to assign new VAR sources with the target of improving VS and reducing the additional VAR sources' cost. While the objective of the lower level is to maintain the overall fuel cost as low as possible. A fuzzy min-max algorithm is used to find the optimum compromise option. An updated IEEE 30-bus test system and a part of the electricity grid in Egypt are used to evaluate the effectiveness of the suggested technique. The results of the presented bi-level optimization approach are compared to those in the literature, indicating the robustness of the suggested technique in addressing the RPP problem. The current study has demonstrated its efficacy in increasing system VS and dealing with network outages involving many lines. It has been proved that using the capacitor bank alone to maximize net savings is better. There is, however, no better way to boost system VS. While FACTS devices are the most effective for increasing system VS, they are also the costliest. It also demonstrates that using a hybrid capacitor bank in conjunction with FACTS to enhance network VS yields good results at a reasonable cost. The results also demonstrate the significance of integrating WTs into power system networks, since this resulted in lower operating costs and higher VS, particularly once their size, location, and optimal coordination with VAR sources are determined.

As a future work, the impact of different renewable energy sources can be studied with other dynamic stability indices and FACTS types.

CRediT authorship contribution statement

Abdelfattah A. Eladl: Data curation, Conceptualization, Validation, Writing – original draft. **Mohamed I. Basha:** Resources, Visualization, Investigation, Software. **Azza A. ElDesouky:** Methodology, Writing – review & editing.

Declaration of Competing Interest

The authors declare that they have no known competing financial interests or personal relationships that could have appeared to influence the work reported in this paper.

Data availability

No data was used for the research described in the article.

References

[1] B. Magalhães, Reactive Power Planning, Porto University, June 2014. PhD. thesis.
[2] A. Salem, A. ElDesouky, A. Farahat, A. Abdelsalam, New analysis framework of Lyapunov- based stability for hybrid wind farm equipped with FRT: a case study of Egyptian grid code, IEEE Access 9 (Jun. 2021) 80320–80339, https://doi.org/10.1109/ACCESS.2021.3085173.
[3] M. Niu, Z. Xu, Reactive power planning for transmission grids with wind power penetration, IEEE PES Innovative Smart Grid Technol. (2012), https://doi.org/10.1109/ISGT-Asia.2012.6303336. Tianjin, China 21–24 May.
[4] A. Salem, A. ElDesouky, A. Alaboudy, New analytical assessment for fast and complete pre-fault restoration of grid-connected FSWTs with fuzzy-logic pitch-angle controller, Int. J. Electr. Power Energy Syst. 136 (2022), https://doi.org/10.1016/j.ijepes.2021.107745.
[5] A. Elmitwally, A. Eladl, J. Morrow, Long-term economic model for allocation of FACTS devices in restructured power systems integrating wind generation, IET Gen. Trans. Dist. 10 (1) (2016) 19–30, https://doi.org/10.1049/iet-gtd.2014.1189. Jan.
[6] L. Chen, J. Zhong, D. Gan, Reactive power planning and its cost allocation for distribution systems with distributed generation, IEEE Power Eng. Soc. General Meeting (2006), https://doi.org/10.1109/pes.2006.1709370. Montreal, Canada, 18–22 June.

[7] Y. Hong, K. Pen, Optimal VAR planning considering intermittent wind power using Markov model and quantum evolutionary algorithm, IEEE Trans. Power Deliv. 25 (4) (2010), https://doi.org/10.1109/TPWRD.2010.2044897.
[8] S. Arefifar, Y. Mohamed, Probabilistic optimal reactive power planning in distribution systems with renewable resources in grid-connected and islanded modes, IEEE Trans. Ind. Electron. 61 (11) (2014), https://doi.org/10.1109/TIE.2014.2308144.
[9] S. Liu, "Research of reactive power planning optimization based on improved adaptive genetic algorithm for wind power plant," 2nd Inter. Conf. on Artificial Intelligence and Industrial Engineering (AIIE 2016) 2016, 10.2991/aiie-16.2016.29.
[10] J. Jing, Z. Yang, Y. Wu, Z. Qian, W. Hu, and X. Jiang, "Optimal planning of reactive power for distribution system considering distributed wind generator," 2nd IEEE Conf. on Energy Internet and Energy System Integration, Beijing, China, 20–22 October 2018, 10.1109/EI2.2018.8582457.
[11] N. Gupta, Stochastic optimal reactive power planning and active power dispatch with large penetration of wind generation, J. Renew. Sustain. Energy 10 (2) (2018), https://doi.org/10.1063/1.5010301.
[12] Z. Wang, H. Liu, and J. Li, "Reactive power planning in distribution network considering the consumption capacity of distributed generation," 5th Asia Conf. on Power and Electrical Engineering (ACPEE), Chengdu, China, 4–7 June 2020, 10.1109/ACPEE48638.2020.9136183.
[13] X. Fang, F. Li, and Y. Xu, "Reactive power planning considering high penetration of wind energy," IEEE PES T&D Conf.and Exposition, Chicago, IL, USA, 14–17 April 2014, 10.1109/tdc.2014.6863471.
[14] S. Mohseni-Bonab, A. Rabiee, B. Mohammadi-Ivatloo, Voltage stability constrained multi-objective optimal reactive power dispatch under load and wind power uncertainties: a stochastic approach, Renew. Energy 85 (2016), https://doi.org/10.1016/j.renene.2015.07.021.
[15] M. Wang and C. Qiu, "Chance-constrained reactive power planning of wind farm integrated distribution system considering voltage stability," 12th IEEE Inter.Conf. on Electronic Measurement and Instruments, ICEMI, Qingdao, China, 16–18 July 2015, vol. 1, 10.1109/ICEMI.2015.7494181.
[16] A. Shojaei, A. Ghadimi, M. Miveh, F. Gandoman, A. Ahmadi, Multiobjective reactive power planning considering the uncertainties of wind farms and loads using information gap decision theory, Renew. Energy 163 (2021), https://doi.org/10.1016/j.renene.2020.06.129.
[17] H. Amaris, M. Alonso, C. Ortega, Reactive power management of power networks with wind generation, Springer-Verlag London 5 (2013), https://doi.org/10.1007/978-1-4471-4667-4.
[18] M. Ghodrati, M. Piri, and S. Sadr, "Probabilistic multi-objective reactive power planning considering large-scale wind integration," International Power System Conf. (PSC), Tehran, Iran, 9–11 December 2019 doi:10.1109/PSC49016.2019.9081501.
[19] N. Karmakar, B. Bhattacharyya, Techno-economic strategy for reactive power planning using Series-shunt compensation in power transmission network, Sust. Energy Tech. Asse 49 (2022), 101677, https://doi.org/10.1016/j.seta.2021.101677. February.
[20] P. Dey, Md. Chowdhury, P. Roy, and T. Aziz, "Developing a methodology for reactive power planning in an industrial microgrid," IEEE Region 10 Symposium (TENSYMP), 1–3 July 2022, Mumbai, India, 10.1109/TENSYMP54529.2022.9864406.
[21] S. Gudadappanavar, S. Mahapatra, Metaheuristic nature-based algorithm for optimal reactive power planning, Int. J. Syst. Assur. Eng. Manag. 13 (3) (2022) 1453–1466, https://doi.org/10.1007/s13198-021-01489-x. June.
[22] V. Gupta1, R. Babu, Reactive power planning problem considering multiple type of FACTS in power systems, Int. J. Syst. Assur. Eng. Manag. 13 (4) (2022) 1885–1894, https://doi.org/10.1007/s13198-021-01588-9. August.
[23] S. Samaan, M. Momeni, M. Knittel, M. Murglat, A. Moser, Multi-criteria based steady-state and dynamic reactive power planning for transmission systems, Elec. Power Syst. Rese 209 (2022), 107929, https://doi.org/10.1016/j.epsr.2022.107929. August.
[24] A. Elmitwally, A. Eladl, Planning of multi-type FACTS devices in restructured power systems with wind generation, Int. J. Electr. Power Energy Syst. 77 (2016) 33–42, https://doi.org/10.1016/j.ijepes.2015.11.023.
[25] A. Eladl, M. Basha, A. ElDesouky, Multi-objective-based reactive power planning and voltage stability enhancement using FACTS and capacitor banks, Electr. Eng. (2022), https://doi.org/10.1007/s00202-022-01542-3.
[26] R. Hemmati, R. Hooshmand, A. Khodabakhshian, Market based transmission expansion and reactive power planning with consideration of wind and load uncertainties, Renew. Sustain. Energy Rev. 29 (2014) 1–10, https://doi.org/10.1016/j.rser.2013.08.062.
[27] M. Ghaljehei, A. Ahmadian, M. Golkar, T. Amraee, A. Elkamel, Stochastic SCUC considering compressed air energy storage and wind power generation: a techno-economic approach with static voltage stability analysis, Int. J. Electr. Power Energy Syst. 100 (2018) 489–507, https://doi.org/10.1016/j.ijepes.2018.02.046.
[28] J. Tian, C. Su, and Z. Chen, "Reactive power capability of the wind turbine with doubly fed induction generator," 39th Annual Conf. of the IEEE Industrial Electronics Society, Vienna, Austria, 10–13 November 2013, doi:10.1109/IECON.2013.6699999.
[29] H. Salama, Voltage stability indices–a comparison and a review, Comp. Elect. Eng. 98 (2022), https://doi.org/10.1016/j.compeleceng.2022.107743.
[30] E. Dehnavi, H. Abdi, Determining optimal buses for implementing demand response as an effective congestion management method, IEEE Trans. Power Syst. 32 (2) (2017), https://doi.org/10.1109/TPWRS.2016.2587843.
[31] S. Ramesh, S. Kannan, S. Baskar, Application of modified NSGA-II algorithm to multi-objective reactive power planning, *Appl. Soft Comput. J.* 12 (2) (2012) 741–753, https://doi.org/10.1016/j.asoc.2011.09.015.
[32] Y. Tang, Voltage Stability Analysis of Power System, Science Press, Springer, 2021, https://doi.org/10.1007/978-981-16-1071-4.
[33] H. Zhang, B. Liu, X. Liu, A. Pahwa, H. Wu, Voltage stability constrained moving target defense against net load redistribution attacks, IEEE Trans. Smart Grid (2022), https://doi.org/10.1109/TSG.2022.3170839.
[34] D. Zhou, U. Annakkage, A. Rajapakse, Online monitoring of voltage stability margin using an artificial neural network, IEEE Trans. Power Syst. 25 (3) (2010) 1566–1574, https://doi.org/10.1109/TPWRS.2009.2038059.
[35] A. Eladl, A. ElDesouky, Optimal economic dispatch for multi heat-electric energy source power system, Int. J. Electr. Power Energy Syst. 110 (2019), https://doi.org/10.1016/j.ijepes.2019.02.040.
[36] Y. Liu, D. Ćetenović, H. Li, E. Gryazina, V. Terzija, An optimized multi-objective reactive power dispatch strategy based on improved genetic algorithm for wind power integrated systems, Int. J. Electr. Power Energy Syst. 136 (2022), https://doi.org/10.1016/j.ijepes.2021.107764.
[37] O. Alsac, B. Stott, Optimal load flow with steady-state security, IEEE Trans. Power Appar. Syst. (3) (1974) 745–751, https://doi.org/10.1109/TPAS.1974.293972. PAS-93.
[38] M. Saravanan, S. Slochanal, P. Venkatesh, J. Abraham, Application of particle swarm optimization technique for optimal location of FACTS devices considering cost of installation and system loadability, Electr. Power Syst. Res. 77 (3–4) (2007) 276–283, https://doi.org/10.1016/j.epsr.2006.03.006.
[39] H. Sultan, O. Kuznetsov, A. Diab, Modelling and performance evaluation of the Egyptian national utility grid based on real data, IEEE Conf. Russ. Young Res. Electr. Electron. Eng. ElConRus (2018) 807–812, https://doi.org/10.1109/EIConRus.2018.8317213, 2018-Janua2018.